Kinetics and Catalysis, Vol. 46, No. 5, 2005, pp. 620–633. Translated from Kinetika i Kataliz, Vol. 46, No. 5, 2005, pp. 660–673.

Structure, Texture, and Acid–Base Properties of Alkaline Earth Oxides, Rare Earth Oxides, and Binary Oxide Systems

A. S. Ivanova

Boreskov Institute of Catalysis, Siberian Division, Russian Academy of Sciences, Novosibirsk, 630090 Russia

Received October 5, 2004

Abstract—The effect of synthesis conditions on the formation of the phase composition, dispersity, pore structure, and acid–base properties of alkaline earth oxides, rare earth oxides, and the Mg–M–O (M = Y, La, or Ce) and Y(La)–M–O (M = Ca, Sr, or Ba) binary systems was studied. It was found that the nature of the system was responsible for the character of phase transformations: the Mg–M–O samples were a mixture of either MgO with Y_2O_3 or MgO with a solid solution based on rare earth oxides ($(LaMg)_2O_3$ or $(CeMg)O_2$); the Y(La)–M–O samples (M = Ca, Sr, or Ba) contained the $M_2Y_2O_5$, MY_2O_4, and MLa_2O_4 compounds, which differ in chemical stability, in addition to La_2O_3 and Y_2O_3 phases. According to XPS data, the M/Mg atomic ratios were much higher than the bulk values; this is indicative of an enrichment of the surface of samples in the second component. An increase in the concentration of M_2O_3 from 5 to 25 mol % resulted in a decrease in the S_{sp} of the Mg–M–O samples from 220 ± 10 to 110 ± 10 m^2/g; the S_{sp} of samples calcined at 750°C was lower by a factor of ~1.5–2. The S_{sp} of the Y(La)–M–O samples was higher than the S_{sp} of individual La_2O_3 and Y_2O_3. The samples were characterized by a biporous texture. The concentrations and strength distributions of surface OH groups, Lewis acid sites, and Lewis base sites depend on the nature and concentration of rare earth elements in the binary samples. The activity of the Mg–M–O samples in the oxidative dehydrogenation reaction of propionitrile correlated with the acid–base surface sites. Among the Ru/Y(La)–M–O catalysts for ammonia synthesis, Ru/Y–Ba–O was the most active; this catalyst provided a higher yield of NH_3 at 250–300°C, as compared with catalysts prepared with the use of other supports (Sibunit, KVU-1, and C/MgO).

INTRODUCTION

Alkaline earth and rare earth oxides and compositions based on these oxides are of increasing current interest. These systems are widely used as catalysts and supports in various chemical reactions. Thus, because of their base properties, they find expanding applications in the oxidative condensation reactions of hydrocarbons [1–9]. In this case, Valenzuela *et al.* [10] found that the activity of binary systems, such as Ca–Ce–O, in the oxidative condensation of ethane was higher than that of individual calcium oxide or cerium oxide. The base properties of MgO also play an important role in the reactions of acrylonitrile synthesis from methanol and acetonitrile [11] and unsaturated ketone hydrogenation [12]. The Fe–Mg–O systems were also used as catalysts for hydrogenation [13–15] and dehydrogenation [16, 17].

Alkaline earth oxides and rare earth oxides are used as supports for metal catalysts (Fe/MgO, Ni/MgO, NiO/CaO, Ru/MgO, and Ni(Ru)/LnO_x (Ln = La, Ce, or Sm)) [18–25]. Boudart *et al.* [20] were the first to study MgO as a support for an iron-containing catalyst for ammonia synthesis. More recently, it was found [21–25] that Ru/MgO catalysts both in the absence and in the presence of promoters ($CsNO_3$, $RbNO_3$, etc.) were much more active in ammonia synthesis than Ru catalysts based on amphoteric or acidic supports (γ-Al_2O_3, SiO_2, activated carbon, etc.). Previously, highly effective Ru catalysts containing rare earth oxides as promoters or supports for ammonia synthesis were reported [26–29].

According to published data [30–32], the active surface sites of alkaline earth oxides and rare earth oxides are ion pairs that consist of valently and coordinatively unsaturated metal and oxygen ions, so-called excitonic centers. An excessive charge on metal and oxygen due to the spatial separation of metals in an active center renders impossible the formation of two metal–oxygen bonds that are equivalent to the bonds in the bulk. The use of UV spectroscopy allowed one to observe directly these centers on the surface of Mg, Ca, and Sr oxides [33, 34]. In particular, upon the removal of CO_3^{2-} and OH groups, the UV spectra of MgO exhibited absorption bands at 270 and 217 nm, which correspond to the $Mg^{2+}(3s^0)O^{2-} \longleftrightarrow Mg^+(3s^1)O^-(2p^5)$ transitions in differently coordinated surface exciton centers [33]. Thus, energetically inhomogeneous surface centers due to an ionic disorder can be the active centers of basic oxides.

It is believed that the introduction of rare earth elements into alkaline earth oxides and vice versa will result in a greater surface ion disorder; this will also affect the distribution of the main surface sites of the

0023-1584/05/4605-0620 © 2005 MAIK "Nauka/Interperiodica"

above systems. This is evidenced by the electronegativity values (E_f) of cations calculated from the equation $E_f = 0.16E_i/r$ (where E_i is the final ionization potential of the cation (eV) and r is the radius of the cation) [35]:

Cation	Ba^{2+}	Sr^{2+}	Ca^{2+}	La^{3+}	Ce^{3+}	Nd^{3+}	Y^{3+}	Mg^{2+}	Zr^{4+}	Ce^{4+}
E_f, nN	1.16	1.47	1.82	2.51	2.69	2.85	3.09	3.25	6.62	6.67

According to the above values, yttrium, lanthanum, and cerium(III) oxides are stronger bases than MgO; however, they are noticeably weaker than CaO, SrO, and BaO in basicity.

Consequently, binary systems based on alkaline earth oxides and rare earth oxides exhibit surface basicity different from that of individual oxides. Therefore, it seemed reasonable to consider the formation of the structure, texture, and acid–base properties of alkaline earth and rare earth oxides and binary systems based on these oxides, namely: Mg–M–O (M = Y, La, or Ce) and Y(La)–M–O (M = Ca, Sr, or Ba).

1. PHYSICOCHEMICAL PROPERTIES OF ALKALINE EARTH OXIDES AND RARE EARTH OXIDES

As a rule, alkaline earth oxides are prepared by the thermal decomposition of various substances:

$$Mg(Ca)CO_3 \xrightarrow{540\text{–}600^\circ C\ (660\text{–}740^\circ C)} MgO + CO_2\ [36, 37];$$

$$Mg(OH)_2 \xrightarrow{380\text{–}430^\circ C} MgO + H_2O\ [38\text{–}41];$$

$$Ca(OH)_2 \xrightarrow{530^\circ C} CaO + CaCO_3 \xrightarrow{830^\circ C} CaO + CO_2\ [42];$$

$$MgCl_2 \longrightarrow MgO + 2HCl\ [43];$$

$$Mg(OR)_2 \xrightarrow{400\text{–}600^\circ C} MgO + \text{gaseous products}\ [44, 45].$$

The above reactions indicate that the temperature of formation of magnesium oxide or calcium oxide depends on the nature of the parent substance. According to Hartman *et al.* [46], hydroxide dehydration occurs with an absorption of heat (ΔH_{298}(MgO) = 81.1 kJ/mol and ΔH_{298}(CaO) = 109.3 kJ/mol). Based on calculated data, Hartman *et al.* [46] determined possible dissociation temperatures to be equal to 358°C for $Mg(OH)_2$ and 504, 540, and 600°C for $Ca(OH)_2$. It was hypothesized that differences in the dissociation temperatures of $Ca(OH)_2$ were due to different preparation conditions.

1.1. Effect of Preparation Conditions on the Properties of Magnesium (Calcium) Hydroxide and Oxide

With the use of magnesium hydroxide as an example, changes in its properties depending on preparation conditions can be illustrated. In the synthesis of a particular composition, attention is focused on the starting raw materials because they affect both the physicochemical properties and the environmental safety of the product. For this purpose, the effects of the nature of parent substances and the synthesis procedure on the properties of magnesium hydroxide and magnesium oxide were studied. Aramendia *et al.* [47] found that the structures of $Mg(OH)_2$ prepared from appropriate substances (Table 1) exhibited certain differences (Fig. 1a), whereas the structures of the oxides prepared by the dehydration of corresponding hydroxides at 600°C were practically identical (Fig. 1b).

Table 1. Effect of the nature of parent substances and preparation procedures on the texture characteristics of MgO calcined in an atmosphere of air at 600°C for 2 h [47]

Sample number	Parent substances and preparation procedure	S_{sp}, m^2/g		V_{pore}, cm^3/g		Average pore diameter, Å	
		$Mg(OH)_2$	MgO	$Mg(OH)_2$	MgO	$Mg(OH)_2$	MgO
1	Commercial $Mg(OH)_2$	13.4	11.5	0.13	0.11	288	347
2	Rehydration of MgO-1	12.3	110.8	0.13	0.32	331	75
3	Precipitation from $Mg(NO_3)_2$	84.8	123.7	0.91	0.84	275	194
4	Precipitation from $MgSO_4$	80.3	162.5	0.64	0.92	217	164
5	Sol–gel method	106.9	39.9	0.54	0.49	127	337
6	Precipitation in the presence of $CO(NH_2)_2$	22.5	100.4	0.15	0.39	226	110
7	Thermal decomposition of $MgCO_3$*	–	–	–	0.42	–	188

* Calcined for 6 h.

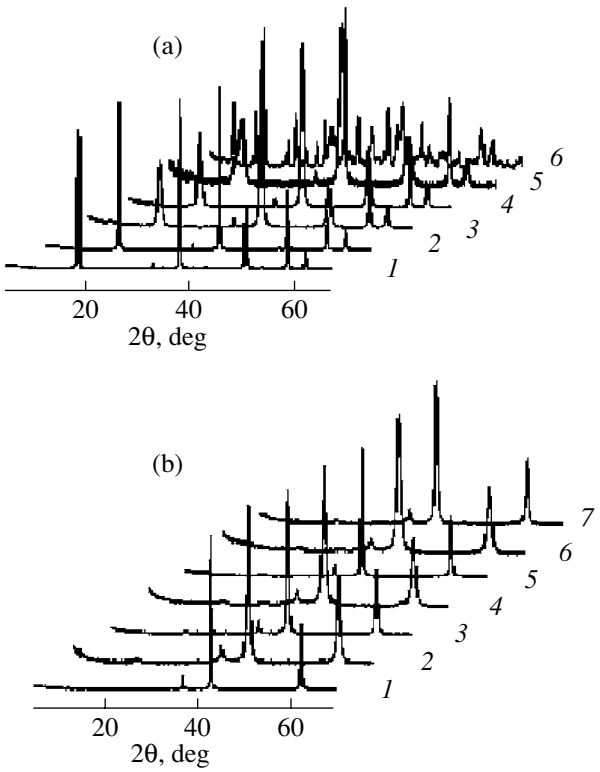

Fig. 1. Diffraction patterns of (a) magnesium hydroxides and (b) magnesium oxides prepared by various procedures [47]. Curve numbers correspond to sample numbers in Table 1.

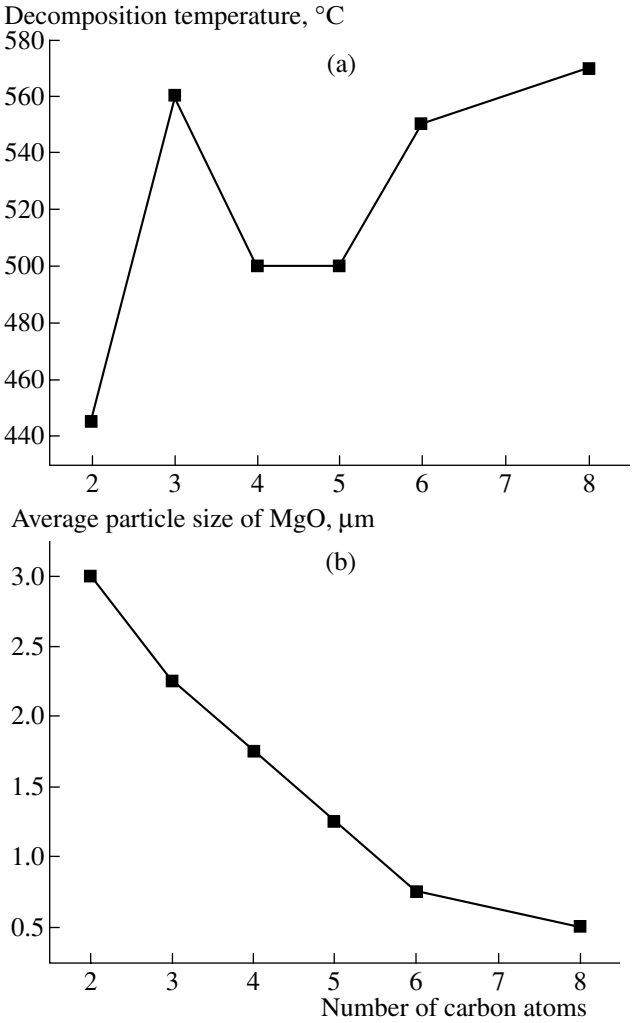

Fig. 2. Dependence of (a) the decomposition temperature of $Mg(OH)_2$ and (b) the particle size of MgO on the number of carbon atoms in magnesium alcoholates [45].

In this case, the texture characteristics of $Mg(OH)_2$ and MgO were different (Table 1). The replacement of magnesium nitrate by magnesium sulfate resulted in an insignificant decrease in the specific surface area (S_{sp}) and pore volume (V_{pore}) of $Mg(OH)_2$. However, on the contrary, the resulting MgO was characterized by greater S_{sp} and V_{pore}. It can be seen (Table 1) that magnesium hydroxide prepared by the sol–gel method was characterized by the greatest value of S_{sp}. It was found [44, 48, 49] that the particle size, morphology, and degree of crystallinity of magnesium hydroxide and magnesium oxide prepared by the sol–gel method can be controlled by selecting an appropriate alcoholate. Thus, magnesium hydroxide with S_{sp} of 700–1000 m^2/g can be prepared by the hydrolysis of $Mg(OCH_3)_2$ under certain conditions [50, 51]. It is likely that the formation of such a surface was due, on the one hand, to the absence of partial hydrolysis products in the presence of which a decrease in the surface area was observed and, on the other hand, to the stabilizing effect of carbon as a constituent of the precipitates. According to published data [50, 51], the formula of magnesium hydroxide can be represented as $MgO_{2.15–2.64}C_{0.41–0.54}H_{2.80–2.95}$. The amount of carbon present in the hydroxide and the temperature of its removal depend on the length of the carbon chain (methyl, ethyl, propyl, etc.) and on the nature of the organic component (propyl, isopropyl, neopentyl, etc.) [45]. It can be seen (Fig. 2a) that the temperature of decomposition of magnesium alcoholates varied from 445 to 560–580°C, which is related to the temperature of decomposition of a corresponding organic fragment [45]. In this case, the particle size of the resulting MgO simultaneously decreased (Fig. 2b). At the same time, MgO prepared by the sol–gel method exhibited the lowest S_{sp} (Table 1); this was likely due to the fact that fine-pore compositions are most prone to agglomeration [38]. To prevent agglomeration, Utamapanya *et al.* [50] recommended performing the thermal treatment of hydroxides under conditions of a dynamic vacuum. According to data in Table 1, magnesium hydroxide samples prepared by precipitation were more thermally stable.

The nature of the precipitating agent also plays an important role in the synthesis of hydroxides by precipitation. Thus, the S_{sp} of $Mg(OH)_2$ precipitated from a nitrate solution with an aqueous NaOH (5 or 10%,

Table 2. Effect of calcination temperature on the structure and texture characteristics of MgO [40]

Treatment temperature, °C	Parameters		S_{sp}, m^2/g	ρ, g/cm^3	D_{ads}, Å
	a, Å	D, Å			
450	4.23	66	350	3.00	57
700	4.22	120	160	3.48	110
1000	4.21	300	40	3.50	430

series I or II, respectively), NH_4OH (25%, series III), or KOH solution (5%, series IV) and dried at 110°C changed in the following manner [40, 41]:

$Mg(OH)_2$	I	II	III	IV
S_{sp}, m^2/g	85	95	40	100

It can be seen that the samples precipitated with NaOH or KOH were characterized by values of S_{sp} higher than that in the precipitation with NH_4OH by a factor of ~2. It was assumed that the incomplete precipitation of magnesium with an ammonia solution could be responsible for the reduced values of S_{sp} in the samples of series III. However, it was found [41] that the amount of $Mg(OH)_2$ formed was practically independent of the nature of the precipitating agent under the chosen synthesis conditions [40, 41]. According to electron-microscopic studies, samples from series III and IV differed in particle size and morphology [41]. The samples precipitated with KOH consisted of plates and needles, which were much smaller than those in precipitates formed with NH_4OH; in the latter case, the plates exhibited a clearly pronounced block structure.

The thermal treatment of $Mg(OH)_2$ from series II at 450°C in a flow of dry air facilitated the formation of highly dispersed oxide, whose S_{sp} was 350 m^2/g (Table 2); the unit cell parameter (a) was equal to 4.23 Å. It is well known [52] that alkaline earth oxides crystallize to form the rock-salt B1 lattice; the coordination number is 6; the unit cell parameters are a_{MgO} = 4.211 Å, a_{CaO} = 4.810 Å, a_{SrO} = 5.140 Å, and a_{BaO} = 5.539 Å. It can be seen in Table 2 that a_{MgO} decreased only after the treatment of a sample at 700–1000°C and became equal to the tabulated value after 1000°C.

As would be expected, the size of coherent-scattering regions (CSRs) (D) increased with treatment temperature; in this case, the value of S_{sp} for MgO decreased from 350 to 40 m^2/g. The particle sizes of MgO determined by X-ray diffraction analysis and calculated from adsorption data were similar (Table 2).

A comparison between data in Tables 1 and 2 demonstrates that MgO calcined in a flow of dry air even at a higher temperature (700°C) was characterized by a higher value of S_{sp} than that in an analogous oxide (Table 1) calcined in an atmosphere of air in a muffle furnace (600°C). At the same time, a change in the atmosphere of calcination had almost no effect on the S_{sp} of alkaline earth oxides (Tables 3, 4) [42, 53].

In turn, the value of S_{sp} for CaO prepared by the thermal treatment of the hydroxide in a flow of dry air changed nonmonotonically (Table 4): as the temperature was increased from 450 to 650°C at the same calcination time (τ = 4 h), a maximum value equal to 36 m^2/g was reached at 550°C. A decrease in τ at the same temperature (550°C) resulted in a decrease in the value of S_{sp} of the resulting product. It is likely that the changes in the value of S_{sp} of the product formed were due to the incomplete decomposition of parent $Ca(OH)_2$. The calcination of $Ca(OH)_2$ in a vacuum allowed us to increase the value of S_{sp} by a factor of ~3.5 as compared with a sample calcined in a flow of air, all other factors being equal (Table 4). According to data on the low-temperature adsorption of nitrogen, CaO calcined in a vacuum exhibited a fine pore structure with an average pore diameter of 116 Å; the fraction of pores with diameters greater than 1000 Å was insignificant [42].

According to current concepts [38], the dispersity of a new phase formed upon the calcination of metal hydroxides depends on the ratio between the rates of formation and growth of the nuclei of this phase. On the assumption that the rate of formation of the nuclei is high, the dispersity depends on the rate of growth. A decrease in the S_{sp} of the product can occur due to the following processes: (1) the bulk agglomeration of oxide particles, which is usually observed at $T > T_{dehydration}$ for the corresponding hydroxide; (2) an

Table 3. Effect of the atmosphere of calcination on the value of S_{sp} for MgO [53]

Atmosphere of calcination	S_{sp}, m^2/g	
	sample C*	sample F
O_2	11.1	8.2
Air	9.5	9.4
N_2	11.6	8.6
He	11.7	9.9

Note: T = 800°C; τ = 1 h; V = 1400 $cm^3\ g^{-1}\ h^{-1}$.

* The sample contained 1.13 wt % Ca and 0.015 wt % Na.

Table 4. Effect of thermal treatment conditions on the S_{sp} of CaO [42]

Calcination conditions	T, °C	τ, h	S_{sp}, m^2/g
In a flow of dry air	450	4	14
	550	1	25
	″	4	36
	650	4	21
In a flow of nitrogen	550	4	36
Under conditions of a dynamic vacuum	″	1	85
	″	1*	70

* The heating rate was 25 K/min; for the other samples, the heating rate was 10 K/min.

increase in the size of crystallites by the coalescence of primary particles, when the removal of water vapor is insufficiently intense; (3) the dehydroxylation of the sample surface to result, in accordance with published data [54], in the formation of oxygen bridges, which close fine pores.

It is likely that the dehydroxylation of an oxide surface was a predominant process in the calcination of $Ca(OH)_2$ under dynamic vacuum conditions at 550°C or in a flow of air at a space velocity of 1000 h^{-1} or higher, when water vapor was rapidly removed [42]. In this case, the degree of decrease in S_{sp} depends on the rate of migration of OH groups rather than the rate of removal of water vapor. We can assume that the rate of migration of OH groups in a vacuum was lower than that in the calcination in a flow of air, and this provided conditions for the formation of a highly dispersed oxide. This is consistent with published data [47, 50, 51]: the high values of S_{sp} (350–500 m^2/g) for MgO can be retained only by the vacuum calcination of the hydroxide prepared by the sol–gel method.

1.2. Effect of Preparation Conditions on the Properties of Rare Earth Hydroxides and Oxides

Rare earth oxides are also prepared either by the dehydration of a corresponding hydroxide or by the decomposition of a carbonate, namely:

$$Y(OH)_3 \xrightarrow{314^\circ C} YOOH \xrightarrow{474^\circ C} Y_2O_3 \text{ [55];}$$

$$Y(OH)_3 \xrightarrow{280^\circ C} YOOH$$

$$\xrightarrow{345^\circ C} Y_2O_3 \cdot H_2O \xrightarrow{530^\circ C} Y_2O_3 \text{ [56];}$$

$$La(OH)_3 \cdot 3H_2O \xrightarrow{120^\circ C} La(OH)_3$$

$$\xrightarrow{380\text{–}400^\circ C} LaOOH \xrightarrow{580^\circ C} La_2O_3 \cdot H_2O \xrightarrow{830^\circ C} La_2O_3 \text{ [57];}$$

$$La_2(CO_3)_3 \cdot 8H_2O \xrightarrow{145\text{–}160^\circ C} La_2(CO_3)$$

$$\xrightarrow{230\text{–}510^\circ C} La_2O_3 \cdot CO_2 \xrightarrow{580\text{–}830^\circ C} La_2O_3 \text{ [58];}$$

$$CeO(OH)_2 \xrightarrow{400^\circ C} CeO_2 \text{ [57].}$$

The character of thermal genesis depends on the preparation procedure. Yttrium and lanthanum hydroxides undergo stepwise dehydration; the hydroxides prepared under hydrothermal conditions [55] or by precipitation [56] are dehydrated in two or three steps, respectively. In this case, yttrium and lanthanum oxides are formed at 530 and 830°C, respectively. The dehydration of cerium hydroxide occurs in a single step, and it is characterized by a lover value of $T_{dehydration}$.

Rare earth oxides differ in crystal structures. Yttrium oxide (Y_2O_3) exhibits a cubic lattice (Mn_2O_3 type) with a = 10.602–10.604 Å [59]. The higher value a = 10.643 Å [56] is characteristic of Y_2O_3 prepared by the treatment of a precipitated hydroxide at 450°C, and only calcination at 700°C facilitates the formation of the oxide with the parameter close to the tabulated value (a = 10.613 Å). The particle size of Y_2O_3 determined by X-ray diffraction analysis was 60 or 100 Å at 450 or 650°C, respectively.

Lanthanum oxide (La_2O_3) forms two main modifications, one of which (low-temperature) is characterized by a hexagonal lattice, and the other (high-temperature) is characterized by a trigonal lattice [60]. The hexagonal modification exhibits a distorted defect structure of the fluorite type with 1/4 vacant positions of oxygen; in this case, the coordination number of lanthanum is equal to 7. The trigonal structure with the lattice parameters a = 3.93–3.94 Å, c = 6.12–6.15 Å, and c/a = 1.56 exhibits ΔH_f^0 = 1795 kJ/mol [61]. The lanthanum oxide prepared by precipitation [56] followed by calcination at 650–700°C exhibits a hexagonal structure with parameters that correspond to tabulated values [59]. The crystallite size (CSR) of La_2O_3 at the specified temperatures varies within the range 250–300 Å.

Cerium forms the following two compounds with oxygen: CeO_2 and Ce_2O_3 [62]. CeO_2 exhibits an fcc lattice of the fluorite (CaF_2) type, *Fm*3*m*; a is 5.4110 [62] or 5.4113 Å [63]; the ionic radius of Ce^{4+} is 0.88 or 1.02 Å according to Belov–Bokii or Goldschmidt, respectively [64]. A special feature of the fluorite structure [65] is that it provides a high stability and effectiveness of the cationic sublattice because of the distribution of all the cations over the points of the closest cubic packing of anions (at the points of the face-centered F lattice); in this case, the oxygen matrix can undergo considerable changes; the coordination number is equal to 8. Ce_2O_3 exhibits a hexagonal lattice of the La_2O_3 type, *P*3*m*1, in which oxygen atoms form the closest cubic packing, and cerium atoms are arranged in octahedral cavities so that two layers are filled and one is empty. The unit cell parameters are equal to a = 3.88 Å and c = 6.06 Å [66] or a = 3.889 Å and c = 6.054 Å [67]; the ionic radius of Ce^{3+} is 1.02 or 1.18 Å according to Belov–Bokii or Goldschmidt, respectively [64]. Ce_2O_3 is unstable in

air; it is usually prepared by the reduction of cerium dioxide.

CeO_2 formed by the dehydration of hydroxide prepared by precipitation and calcined at 450°C exhibits a cubic structure with a = 5.411 Å [57], which is practically equal to the tabulated parameter [59]. The particle size (CSR) of CeO_2 prepared at 400 or 700°C is 400 or 500 Å, respectively.

The value of S_{sp} for rare earth oxides depends on the synthesis conditions of the corresponding hydroxides. Lanthanum oxide prepared by the treatment of hydroxide precipitated at room temperature exhibits S_{sp} smaller than that in the case of hydroxide precipitated at 70°C by a factor of ~4 (Table 5). The conditions of precipitation affect the S_{sp} of cerium oxide to a smaller extent. Among the above oxides, yttrium oxide is the most thermally stable (Table 5).

Table 5. Effect of preparation conditions on the S_{sp} of rare earth oxides

Oxide	Temperature of hydroxide precipitation, °C	S_{sp}, m^2/g	
		400°C	700°C
Y_2O_3	~23	90	90
La_2O_3	~23	22	16
	70	80	40
CeO_2	~23	97	30
	70	75	25

2. PHYSICOCHEMICAL PROPERTIES OF THE Mg–M–O (M = Y, La, Ce) AND Y(La)–M–O (M = Ca, Sr, Ba) BINARY SYSTEMS

Binary compositions based on magnesium oxide or yttrium (lanthanum) oxides were prepared by precipitation from a mixed solution of corresponding nitrates with 2 N KOH at a specified pH and temperature followed by filtration, washing, drying, and thermal treatment.

2.1. Phase Composition of Binary Systems

2.1.1. Phase composition of binary systems based on MgO. A study of the phase composition of Mg–M–O samples demonstrated that it depends on the nature of the rare earth element and on the temperature of treatment. Because the ionic radii of added components ($r_{Y^{3+}} = 0.97$, $r_{La^{3+}} = 1.22$, and $r_{Ce^{4+}} = 0.88$ Å) are greater than the ionic radius of the main component ($r_{Mg^{2+}} = 0.74$ Å), the probability of formation of a solid solution based on magnesium oxide is minimal. Indeed, the following phases were formed depending on the fraction of a rare earth element (mol %) introduced into MgO and on the calcination temperature:

$$\text{Mg–Y(<10)–O} \xrightarrow{450^\circ\text{C}} \text{MgO}$$

$$+ \text{ amorphous phase} \xrightarrow{750^\circ\text{C}} \text{MgO} + Y_2O_3,$$

$$\text{Mg–Y(>10)–O} \xrightarrow{450^\circ\text{C}} \text{MgO} + Y_2O_3 \xrightarrow{750^\circ\text{C}} \text{MgO} + Y_2O_3,$$

$$\text{Mg–La(<20)–O} \xrightarrow{450^\circ\text{C}} \text{amorphous phase}$$

$$\xrightarrow{750^\circ\text{C}} \text{MgO} + La_2O_3 + La_2MgO_x,$$

$$\text{Mg–Ce(}\leq 25\text{)–O} \xrightarrow{450^\circ\text{C}} \text{MgO}$$

$$+ (Ce,Mg)O_2 \xrightarrow{750^\circ\text{C}} \text{MgO} + (Ce,Mg)O_2.$$

The reaction product observed in the Mg–La(Ce)–O systems was a solid solution based on La_2O_3 and CeO_2; no interaction occurred in the Mg–Y–O system. The presence or absence of interactions in the test systems can be due to the positions of corresponding components in the electronegativity series (see above). A comparison between electronegativity values indicates that the differences between these values for the Mg–La–O and Mg–Ce–O systems are 0.74 and 3.42 nN, respectively, whereas this difference for Mg–Y–O is 0.16 nN; that is, the greater ΔE_f, the more probable the interaction between components.

2.1.2. Phase composition of binary systems based on $Y(La)_2O_3$. Because of differences in the formation of $Y(La)_2O_3$ and CeO_2 oxides, the Y_2O_3 and La_2O_3 oxides were chosen for studying the effect of the nature of the alkaline earth metal on the physicochemical properties of the Y(La)–M–O systems (M = Ca, Sr, Ba). It was found [56] that Y(La)–M–O samples containing 5–9 mol % MO are mixtures of the following phases depending on temperature:

$$\text{Y–Ca(Sr)–O} \xrightarrow{450^\circ\text{C}} Y_2O_3$$

$$+ Ca(Sr)_2Y_2O_5 \xrightarrow{650^\circ\text{C}} Y_2O_3 + \text{Ca(Sr)O},$$

$$\text{Y–Ba–O} \xrightarrow{450^\circ\text{C}} Y_2O_3 + BaY_2O_4$$

$$+ BaCO_3 \xrightarrow{650^\circ\text{C}} Y_2O_3 + BaCO_3,$$

$$\text{La–M–O} \xrightarrow{450^\circ\text{C}} \text{amorphous phase} \xrightarrow{650^\circ\text{C}} La_2O_3 + MLa_2O_4.$$

Consequently, Y(La)–M–O binary compositions contain reaction products ($M_2Y_2O_5$, MY_2O_4, and MLa_2O_4), which differ in thermal stability, along with individual La_2O_3 or Y_2O_3 phases. As would be expected, the crystallite size of the above compounds determined by X-ray diffraction analysis was much smaller than that of Y_2O_3 or La_2O_3 crystallites prepared under analogous conditions. On this basis, higher val-

ues of S_{sp} would be expected, as compared with corresponding individual oxides.

2.2. Texture Characteristics of Binary Systems

Figure 3 shows changes in the value of S_{sp} in Mg–M–O binary samples calcined at 450°C. It can be seen that the addition of ~5 mol % M_2O_3 to MgO had almost no effect on the S_{sp} of the binary samples. An increase in the M_2O_3 content of Mg–M–O was accompanied by a decrease in S_{sp}. The observed changes in S_{sp} were due to phase transformations in binary systems: the fraction of a phase based on M_2O_3, whose S_{sp} is lower than the S_{sp} of MgO (Tables 2, 5), increased with the fraction of M_2O_3 in Mg–M–O. An increase in the temperature of sample treatment to 750°C also facilitated a decrease in S_{sp} by a factor of ~1.5–2.

In contrast, the values of S_{sp} for Y(La)–M–O binary compositions calcined at 450°C were higher than the values of S_{sp} for individual Y_2O_3 and La_2O_3 prepared under analogous conditions, namely [56]:

Samples:	Y_2O_3	Y–Ca–O	Y–Sr–O	Y–Ba–O	La_2O_3	La–Ca–O	La–Sr–O	La–Ba–O
S_{sp} (450°C), m^2/g	90	130	100	110	45	85	95	110
S_{sp} (650°C), m^2/g	90	115	76	57	40	48	43	31

Moreover, S_{sp} for samples based on Y_2O_3 was higher than that for samples based on La_2O_3. An increase in $T_{calcination}$ to 650°C had almost no effect on the values of S_{sp} for individual Y_2O_3 and La_2O_3 oxides; however, it resulted in a decrease in this value for binary compositions. As a result, the values of S_{sp} for binary oxides after calcination at 650°C were comparable to or even lower than the S_{sp} of Y_2O_3 or La_2O_3 in all cases except for M = Ca.

According to data on the low-temperature adsorption of nitrogen, Mg–M–O binary samples containing 5 mol % M_2O_3 and calcined at 450°C were characterized by a biporous structure: the total pore volume decreased from 0.66 ⟶ 0.50 ⟶ 0.48 cm^3/g in the order Mg–Y–O ⟶ Mg–La–O ⟶ Mg–Ce–O, respectively. The average pore diameter decreased in the same order, namely: 160 ⟶ 134 ⟶ 115 Å, respectively.

2.3. Surface Properties of Binary Compositions

The surface properties of samples were studied by X-ray photoelectron spectroscopy (XPS) and the IR spectroscopy of adsorbed CO and deuterochloroform molecules.

To determine the possible states of yttrium, lanthanum, and cerium in Mg–M–O samples (M = Y, La, or Ce) containing ~5 mol % M_2O_3 calcined at 450°C, the XPS spectra were measured (Fig. 4). An analysis of the results demonstrated that carbonates were present on the surface of samples in addition to the main components: a peak at E_b = 288.9 eV in the C1*s* spectrum corresponds to carbonates [68, 69]. The O1*s* spectrum exhibited two peaks at E_b = 529.4–529.6 and 531.1–531.5 eV; the former peak was due to the lattice oxygen of Mg–O, and the latter peak was due to magnesium carbonate and the corresponding rare earth carbonate [70]. Both of the peaks were shifted toward lower values of E_b, as compared with individual MgO. The values of M3*d* E_b are 156.0, 833.8, and 881.1 eV for yttrium–, lanthanum–, and cerium–magnesium samples, respectively (Fig. 5), which are lower than the values of M3*d* E_b for individual oxides (Table 6). This shift can be due to the fact that oxygen atoms in the near-surface layers of Mg–M–O exhibit more pronounced base properties, as compared with oxygen atoms in MgO.

It can be seen in Table 6 that the surface concentrations of lanthanum and cerium were similar, whereas the surface concentration of yttrium was much higher. This may be due to the absence of interactions between components in the Mg–Y–O system; correspondingly, the surface concentration of yttrium was higher. With consideration for the fact that the volume ratios in these samples increased in the order 0.061 (La/Mg) < 0.078 (Y/Mg) < 0.085 (Ce/Mg), a comparison between these values and data in Table 6 suggests an enrichment of the surfaces with rare earth elements. The overall stoichiometry (O/M and O/Mg after deduction of the contribution of surface carbonate groups) suggests (Table 6) that the surface concentration of oxygen reached a maximum in the Mg–La–O system.

The state of Mg in the Mg–M–O systems was evaluated from the modified Auger parameter α(Mg), which is the sum of E_b of the Mg1*s* core level and the kinetic energy of the corresponding Auger peak Mg*KLL*. In the case of Mg–Y(Ce)–O, the value of α(Mg) was equal to 2484.8 eV, which is close to the Auger parameter found for MgO: α(Mg) = 2485.1 eV. In the case of Mg–La–O, the value of α(Mg) was 2483.5 eV, which is smaller than that for MgO by 1.6 eV. This difference is indicative of another electronic state and/or local environment of magnesium ions in the near-surface layers of Mg–La–O, as compared with pure MgO.

We measured IR spectra in order to determine the acid–base properties of the test samples. Figure 6 shows the spectra of OH groups in binary samples cal-

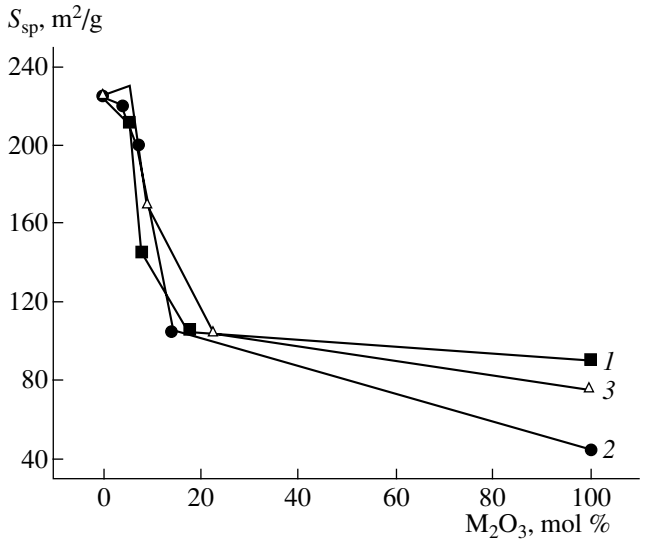

Fig. 3. The specific surface area of magnesium-containing binary samples calcined at 450°C: (*1*) Mg–Y–O, (*2*) Mg–La–O, and (*3*) Mg–Ce–O.

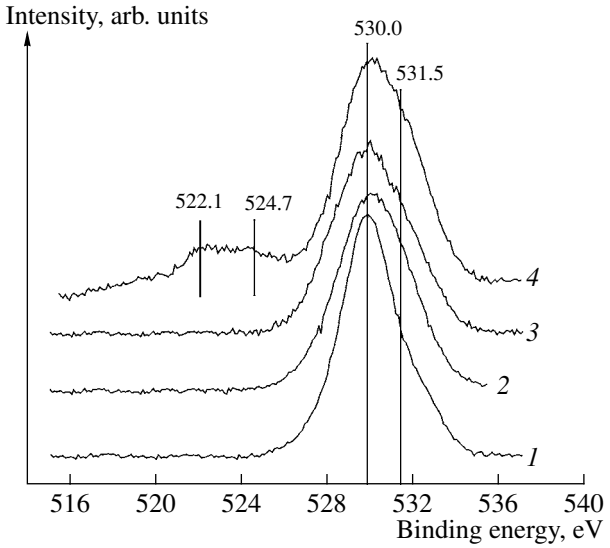

Fig. 4. O1*s* spectra of (*1*) MgO and Mg–M–O binary systems (≈5 mol % M_2O_3; M = (*2*) Y, (*3*) Ce, or (*4*) La) calcined at 450°C.

cined at 450°C, and Table 7 summarizes the measured concentrations of these groups.

All of the samples exhibited an absorption band at 3756 cm^{-1}; MgO exhibited an absorption band at 3760 cm^{-1}; this absorption band belongs to terminal OH groups. Note that OH groups on MgO are somewhat different from the well-known groups [71, 72]: usually, absorption bands at 3745–3755 cm^{-1} were observed on the surface of MgO; a difference of 5–10 cm^{-1} is sufficient for asserting a specific character of the sample; however, the nature of this specific character is unclear. The position of this absorption band in Mg–M–O samples remained practically unchanged (Fig. 6); however, the concentration of OH groups depends on the nature and fraction of rare earth elements (Table 7). Depending on the nature of the rare earth element, it increased in the order Mg–Y (5%)–O < Mg–O < Mg–Ce (5%)–O ≈ Mg–La(5%)–O.

In addition to the absorption band at 3756 cm^{-1}, the spectra of Mg–La–O samples exhibited absorption bands at 3522, 3548, and 3627 cm^{-1}, which may correspond to OH groups bound to hydroxocarbonate fragments. Indeed, carbonates in high concentrations were detected in these samples (Fig. 7), as evidenced by the absorption bands at 1080, 1370–1540, and 1700–1850 cm^{-1}, which belong to symmetric vibrations, antisymmetric vibrations, and the vibrations of terminal surface CO fragments, respectively. The concentration of carbonate groups was estimated at ~900–3000 μmol/g.

Figure 8a shows the IR spectra of CO measured at a CO pressure of 10 Torr. A broad band with a maximum at about 2150 cm^{-1} was observed. In this region, the vibrations of physically adsorbed CO molecules and CO molecules bound to very weak Lewis acid sites (LASs) and weakly acidic OH groups are detected. Because no interaction of OH groups (absorption band at 3756 cm^{-1}) with CO was observed, it is believed that only weak LASs occurred on the surface of the samples. We failed to determine the concentration of these sites because it is impossible to separate correctly physical adsorption and weak coordination. Figure 8b shows the IR spectra of CO measured at a pressure of 0.1 Torr. In this case, we were able to distinguish a small amount of stronger LASs, which were characterized by absorption bands at 2200 and 2190–2196 cm^{-1}. These sites are typical of coordinatively unsaturated Mg^{2+} ions [73]. The concentration of the above sites varied over the range 0.8–7.0 μmol/g and, depending on the nature of rare earth elements, increased in the order Mg–O < Mg–Ce–O < Mg–Y–O < Mg–La–O. In addition to strong LASs, weaker LASs occurred on the

Table 6. Chemical composition of surface layers determined from XPS data for binary samples calcined at 450°C

Sample	M3$d_{5/2}$ E_b, eV	M_2O_3 M3$d_{5/2}$ E_b, eV	[M]/[Mg]	[O]/[Mg]	[O]/[M]
Mg–Y–O	156.0	156.8	0.172	1.58	9.2
Mg–La–O	833.8	834.4	0.097	2.00	20.6
Mg–Ce–O	881.1	882.0	0.109	1.66	15.2

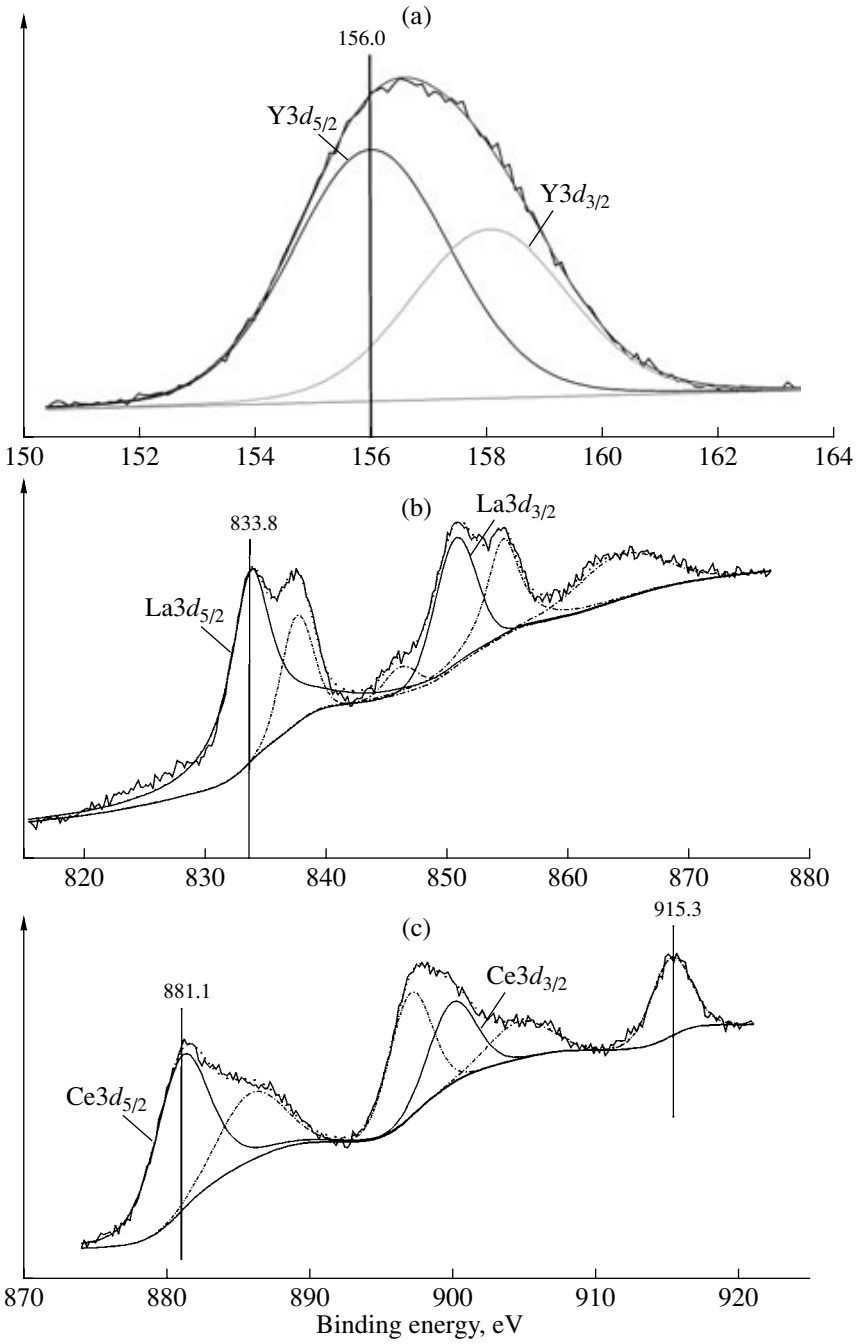

Fig. 5. M3*d* spectra of binary systems calcined at 450°C: (a) Mg–Y–O, (b) Mg–La–O, and (c) Mg–Ce–O. Broken curves indicate satellite lines.

surface of the test samples, which were characterized by absorption bands at 2163–2165 and 2177 cm^{-1}, respectively (Fig. 8b). The concentration of these weak LASs increased in the order Mg–O (2.6 μmol/g) < Mg–Ce–O (13.2 μmol/g) < Mg–La–O (15 μmol/g) < Mg–Y–O (27 μmol/g); that is, the concentration of weak LASs in the Mg–Y–O system was higher than the concentration of strong LASs by one order of magnitude.

Figure 9 shows the spectra of adsorbed deuterochloroform. Three types of basic sites were observed in MgO (Fig. 9); these sites are characterized by bands at 2255 (weak), 2225 (medium-strength), and 2156 cm^{-1} (strong). According to published data [53], they were due to the adsorption of deuterochloroform at OH groups, O, and O^{2-}, respectively. An intense absorption maximum at 2231–2236 cm^{-1} broadened toward low frequencies can also be seen in the spectra of Mg–M–O

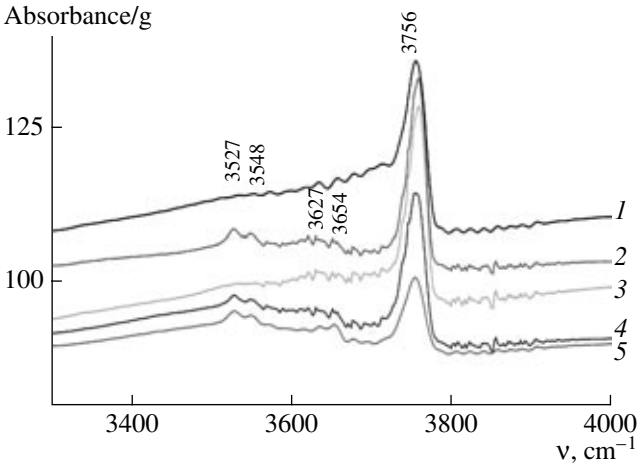

Fig. 6. IR spectra of OH groups: (*1*) Mg–Y(5.0)–O, (*2*) Mg–La(5.0)–O, (*3*) Mg–Ce(5.0)–O, (*4*) Mg–La(7.3)–O, and (*5*) Mg–La(14.3)–O.

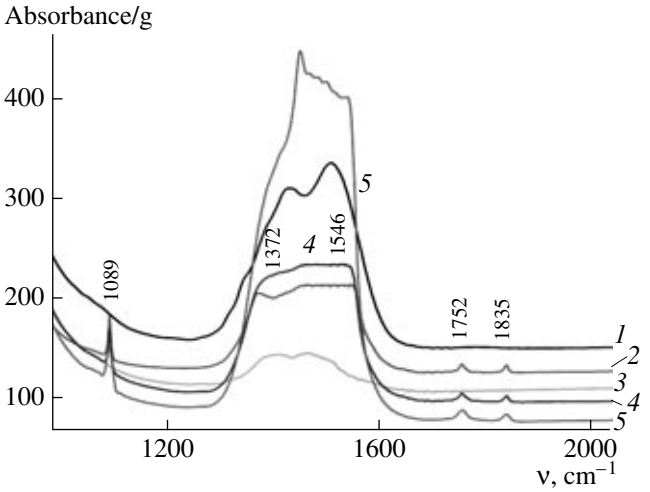

Fig. 7. IR spectra in the region of carbonate groups: (*1*) Mg–Y(5.0)–O, (*2*) Mg–La(5.0)–O, (*3*) Mg–Ce(5.0)–O, (*4*) Mg–La(7.3)–O, and (*5*) Mg–La(14.3)–O.

samples (Fig. 9). Two components at about 2210–2225 and 2167–2185 cm^{-1} can be additionally separated as a result of spectra deconvolution. These components correspond to stronger basic sites. An analysis of quantitative data demonstrated (Table 8) that the addition of ~5 mol % M_2O_3 to MgO was favorable for an increase in the basicity of binary samples because absorption bands due to weak and medium-strength basic sites shifted toward smaller values. However, this trend was not observed for strong basic sites. They were likely blocked by adsorbed carbonates, which were detected in both XPS and IR spectra. Nevertheless, the total concentration of basic sites increased depending on the nature of rare earth elements (Table 8): Mg–Y(5)–O < Mg–Ce(5)–O < Mg–La(5)–O. The dependence found is consistent with published data [74]: the addition of a small amount of lanthanum (which is less basic than calcium) to CaO decreased the basicity of the binary composition, whereas the presence of strontium (which is more basic than calcium) increased the basicity; that is, the basicity increased in the order Ca–La–O < CaO < Ca–Sr–La–O.

An increase in the temperature of sample treatment was accompanied by a redistribution of basic sites. In particular, the surface concentration of basic sites (%) in MgO was distributed, depending on temperature, as follows:

	Weak	Medium	Strong	
MgO (450°C)	9	53	38	[This work]
MgO (600°C)	13	36	51	[47]

That is, as the temperature was increased, medium-strength and strong basic sites mainly underwent a redistribution on the surface of MgO. According to published data [53], the surface basicity of MgO depends on not only temperature but also the atmosphere of calcination. According to the results given in Table 9, samples calcined in an atmosphere of oxygen were characterized by the lowest concentration of basic sites, whereas the highest concentrations were observed in samples **C** and **F** calcined in air and helium atmospheres, respectively. Kus *et al.* [53] related the above differences to different interactions of gas-phase molecules with the surface (**F**-centers) of the oxide.

Thus, a study of the acid–base properties of MgO and Mg–M–O samples demonstrated that the addition of rare earth elements (Y, La, and Ce) resulted in an increase in the concentration of strong basic sites in the binary systems. Moreover, the strength distribution of basic sites can also be regulated by changing the temperature and atmosphere of calcination.

Because differences in the acid–base properties of binary systems can affect the activity of catalysts based

Table 7. Positions of absorption band maximums due to the hydroxyl groups of magnesium-containing samples calcined at 450°C

Sample*	ν(OH), cm^{-1}	Concentration of OH groups, μmol/g
Mg–O	3760	180
Mg–Y(5.0)–O	3756	160
Mg–La(5.0)–O	3756	220
Mg–La(7.3)–O	3756	170
Mg–La(14.3)–O	3756	85
Mg–Ce(5.0)–O	3756	220

* The concentration of the second component (in mol %) is given in parentheses.

Table 8. Positions of C–D bands due to adsorbed $CDCl_3$ and the concentrations of basic sites

Sample	ν, cm^{-1} (N, μmol/g)					
	weak		medium		strong	
MgO	2255	(100)	2225	(580)	2156	(410)
Mg–Y(5)–O	2240	(150)	2219	(150)	2168	(33)
Mg–La(5)–O	2235	(385)	2210	(230)	2166	(65)
Mg–Ce(5)–O	2234	(200)	2212	(105)	2177	(55)

on alkaline earth and rare earth oxides, we exemplified the efficiency of binary compositions, as compared with individual oxides, using two reactions.

2.4. Catalytic Properties of Binary Systems

2.4.1. Oxidative dehydrogenation of propionitrile. Acrylonitrile, ethylene, and carbon oxides were the main reaction products on the test samples (Table 10); methane and acetonitrile were formed in smaller amounts (maximum selectivities for these products did not exceed 10%). The conversion of propionitrile occurred with a detectable rate at $T >$ 600°C.

Figure 10 shows the temperature dependence of the conversion of propionitrile and the selectivities for reaction products on a Mg–La(4.1)–O sample. The conversion of propionitrile monotonically increased over the test temperature range. The selectivities for cracking products increased with $T_{reaction}$, whereas the selectivities for deep oxidation products decreased. The selectivity for acrylonitrile initially increased (up to 700°C) and then gradually decreased. The observed behaviors were due to the simultaneous occurrence of the dehydrogenation, cracking, and oxidation of propionitrile.

The activity of samples was evaluated from the constant of the overall conversion of propionitrile, which was calculated by the first-order equation $k = -\ln(1 - x)/\tau$, where x is the conversion of propionitrile, and τ is the contact time. Table 10 summarizes the constants of the overall conversion of propionitrile and the yields of

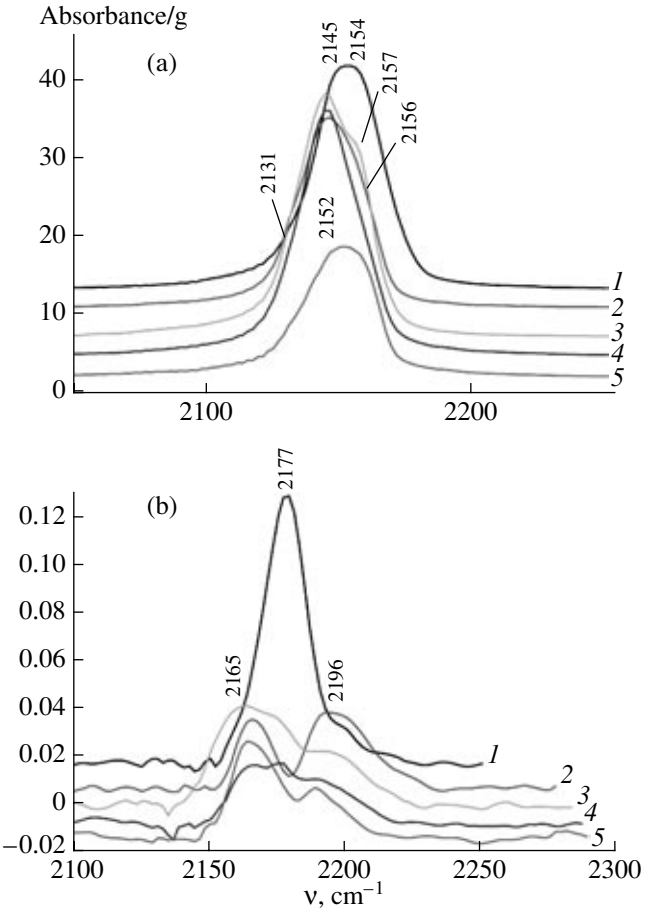

Fig. 8. IR spectra of CO adsorbed at 196°C and a pressure of (a) 10 or (b) 0.1 Torr: (*1*) Mg–Y(5.0)–O, (*2*) Mg–La(5.0)–O, (*3*) Mg–Ce(5.0)–O, (*4*) Mg–La(7.3)–O, and (*5*) Mg–La(14.3)–O.

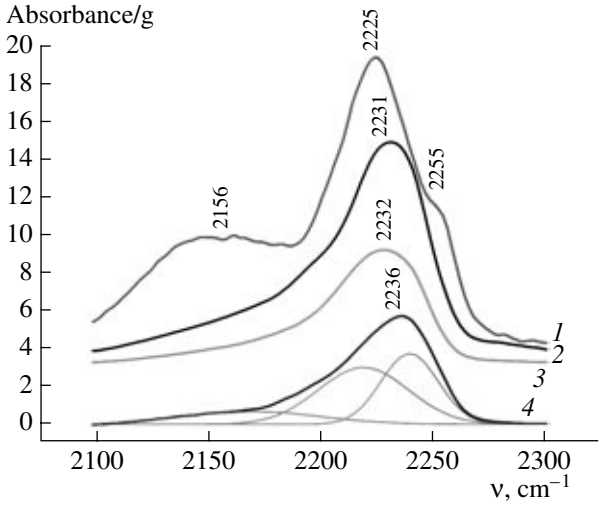

Fig. 9. IR spectra of deuterochloroform adsorbed at room temperature on the following systems: (*1*) MgO, (*2*) Mg–La(5.0)–O, (*3*) Mg–Ce(5.0)–O, and (*4*) Mg–Y(5.0)–O.

Table 9. Effect of calcination atmospheres on the basic properties of MgO calcined at 630°C for 3 h [53]

Sample*	Calcination atmosphere	Concentration of basic sites, μmol/m^2				
		weak	medium	strong	very strong	Σ
C	He	2.7	2.8	1.3	2.1	9.0
	Air	2.8	3.1	1.7	2.7	10.3
	O_2	1.6	2.3	1.3	2.1	7.3
F	He	4.1	2.3	0.4	0.2	7.0
	Air	3.9	1.8	0.3	0.2	6.2
	O_2	4.0	1.6	0.3	0.1	6.0

* Sample **C** contained 1.13 wt % Ca and 0.015 wt % Na; sample **F** contained <0.02 wt % Ca and <0.01 wt % Na.

acrylonitrile ($Y_{acrylonitrile}$) measured at 700°C. The values of k varied over a range of 0.4–0.7, ~1, or ≥1 s^{-1} for samples based on La_2O_3, Y_2O_3, or MgO, respectively. In this case, the greatest yield of acrylonitrile (30–32%) was observed on Mg–M–O samples, among which Mg–Y–O was most active (Table 8), namely:

k, s^{-1} Mg–Y–O > Mg–Ce–O > Mg–La–O

Yield of acrylonitrile Mg–Y–O > Mg–Ce–O > Mg–La–O.

With consideration for the corresponding changes in the concentrations of acid (LAS) and basic sites (BS), as noted above, the following relations were observed in magnesium-containing samples:

ΣBS Mg–Y–O < Mg–Ce–O < Mg–La–O

$LAS_{2165–2177}$, μmol/g 2.07 > 13.2 15.0.

That is, the total concentration of basic sites increased in the above order, whereas the concentration of weak LASs decreased.

Thus, a maximum efficiency of the conversion of propionitrile into acrylonitrile in the test reaction was observed on a Mg–Y–O sample, which is likely characterized by an optimum ratio between acid and basic sites of a certain strength.

2.4.2. Low-temperature ammonia synthesis. The results of testing Ru/Y(La)–M–O catalysts demonstrated [56] that the rate of ammonia formation increased upon the replacement of Y_2O_3 and La_2O_3 oxides by Y(La)–M–O– binary compositions. With the use of Y–M–O systems as supports, the activity of catalysts at 300 and 350°C increased in the order Y–Ca–O < Y–Sr–O < Y–Ba–O, that is, in the same order as the basicity of MO increased (Fig. 11).

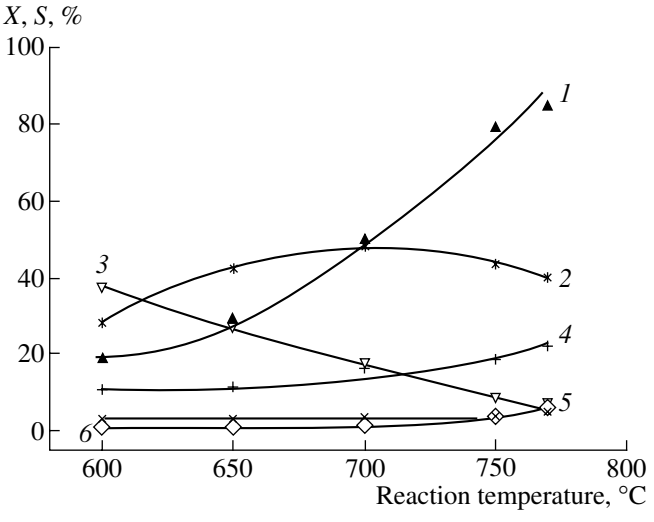

Fig. 10. Dependence of (*1*) propionitrile conversion and selectivities for (*2*) acrylonitirle, (*3*) carbon monoxide, (*4*) ethylene, (*5*) methane, and (*6*) acetonitrile on the temperature of reaction on the Mg–La(5.0)–O sample.

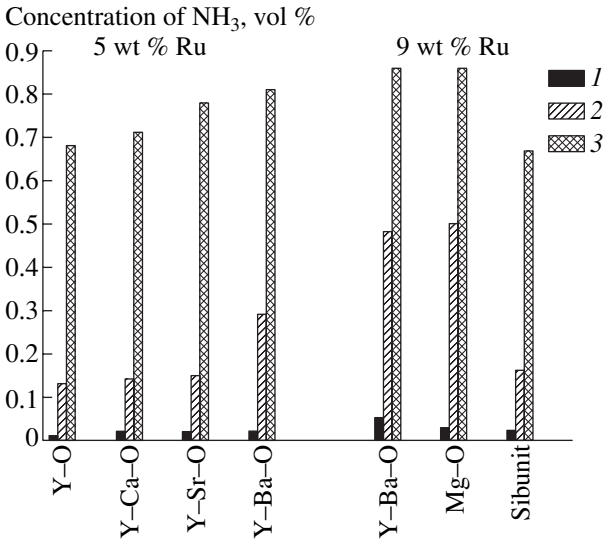

Fig. 11. Steady-state concentration of ammonia in a gas flow depending on the nature of the support and the concentration of ruthenium. T = (*1*) 250, (*2*) 300, or (*3*) 350°C.

Table 10. Catalytic properties of samples in the oxidative dehydrogenation reaction of propionitrile ($T_{reaction}$ = 700°C)

No.	Sample	K, s^{-1}	$Y_{acrylonitrile}$, %
1	Y_2O_3	0.5	19.0
2	La_2O_3	0.4	11.2
3	Y–Ca(5.5)–O	0.9*	19.7
4	Y–Ba(6.2)–O	1.0*	20.4
5	La–Ca(9.3)–O	0.7	22.4
6	La–Ba(4.3)–O	0.6	24.9
7	Mg–Y(5.6)–O	2.8	31.7
8	Mg–La(4.1)–O	0.9	23.4
9	Mg–Ce(5.7)–O	1.4	29.7
10	Mg–Ce(23)–O	2.2	30.0

* $T_{reaction}$ = 650°C.

Thus, among the catalysts under consideration, Ru/Y–Ba–O (5 wt % Ru) was the most efficient catalyst in the reaction of low-temperature ammonia synthesis. Its activity can be improved by increasing Ru content to 9 wt % (Fig. 11): the steady-state concentration of ammonia in a gas flow at 250 or 300°C was as high as 0.05 or 0.48 vol %, respectively, whereas the process of ammonia synthesis reached an equilibrium at 350 and 400°C. The resulting Ru/Y–Ba–O catalyst was far superior to analogous ruthenium catalysts on Sibunit [75], KVU-1 [24], and carbonized MgO [76] in activity at 250–300°C and to a catalyst on MgO at 250°C [24].

REFERENCES

1. Keller, G.E. and Bhasin, M.M., *J. Catal.*, 1982, vol. 73, p. 9.
2. Otsuka, K., Jinno, K., and Morikawa, A., *J. Catal.*, 1986, vol. 100, p. 353.
3. Sofranko, J.A., Leonard, J.J., and Jones, C.A., *J. Catal.*, 1987, vol. 103, p. 302.
4. Matsuda, N., Ohyachi, K., and Matsuura, I., *Chem. Express*, 1990, vol. 5, no. 8, p. 533.
5. Choudhary, V.R. and Rane, V.H., *J. Catal.*, 1991, vol. 130, no. 2, p. 411.
6. Krylov, O.V., *Usp. Khim.*, 1992, vol. 61, p. 1550.
7. Ivanova, A.S., Moroz, E.M., and Litvak, G.S., *React. Kinet. Catal. Lett.*, 1998, vol. 65, no. 1, p. 169.
8. Ivanova, A.S., Paukshtis, E.A., Sobyanin, V.A., and Galvita, V.V., *React. Kinet. Catal. Lett.*, 1998, vol. 64, no. 2, p. 337.
9. Yu, L., Li, W., Ducarme, V., Mirodatos, C., and Martin, G.A., *Appl. Catal., A*, 1998, vol. 175, p. 173.
10. Valenzuela, R.Y., Bueno, G., Solbes, A., Sabifia, F., Martinez, E., and Corberan, V.C., *Top. Catal.*, 2001, vol. 15, nos. 2–4, p. 181.
11. Jackson, S.D., Kelly, G.J., Hamilton, Ch.A., and Davies, L., *React. Kinet. Catal. Lett.*, 2003, vol. 79, no. 2, p. 213.
12. Szollosi, G. and Bartok, M., *J. Mol. Catal. A*, 1999, vol. 148, nos. 1–2, p. 265.
13. Topsoe, H., Dumesic, J.A., Derouane, E.G., Clausen, B.S., Morup, S., Villadsen, J., and Topsoe, N., *Stud. Surf. Sci. Catal.*, 1979, vol. 3, p. 365.
14. Shen, J., Guang, B., Tu, M., and Chen, Y., *Catal. Today*, 1996, vol. 30, nos. 1–3, p. 77.
15. Gallegos, N.G., Alvarez, A.M., Cagnoli, M.Y., Bengoa, J.F., Marchetti, S.G., Mercador, R.C., and Veramian, A.A., *J. Catal.*, 1996, vol. 161, p. 132.
16. Kock, A.J.H.M., Fortuin, H.M., and Geus, J.W., *J. Catal.*, 1985, vol. 96, p. 261.
17. Stobbe, D.E., van Buren, F.R., Stobbe-Kreemers, A.W., van Dillen, A.J., and Geus, J.W., *J. Chem. Soc., Faraday Trans.*, 1991, vol. 87, p. 1631.
18. Ivanova, A.S., Bobrova, I.I., Moroz, E.M., Gavrilov, V.Yu., Kalinkin, A.S., and Sobyanin, V.A., *Kinet. Katal.*, 1993, vol. 34, no. 4, p. 758.
19. Tang, S., Lin, J., and Tan, K.L., *Catal. Lett.*, 1998, vol. 51, p. 169.
20. Boudart, M., Delbouille, A., Dumesic, J.A., Khammouma, S., and Topsoe, H., *J. Catal.*, 1975, vol. 37, p. 486.
21. Murata, S. and Aika, K., *J. Catal.*, 1992, vol. 136, no. 1, p. 110.
22. Khaja, M.S., *Indian J. Chem., Sect. A*, 1993, vol. 32, no. 4, p. 383.
23. Shur, V.B. and Yunusov, S.M., *Izv. Akad. Nauk, Ser. Khim.*, 1998, no. 5, p. 796.
24. Yunusov, S.M., Moroz, B.L., Ivanova, A.S., Likholobov, V.A., and Shur, V.B., *J. Mol. Catal. A*, 1998, vol. 132, no. 3, p. 263.
25. Aika, K. and Tamary, K., *Ammonia: Catalysis and Manufacture*, Nielsen, A., Ed., Berlin: Springer, 1995, p. 104.
26. Aika, K., Takano, T., and Murata, S., *J. Catal.*, 1992, vol. 136, no. 1, p. 126.
27. Murata, S. and Aika, K., *J. Catal.*, 1992, vol. 136, no. 1, p. 118.
28. Kadowaki, S. and Aika, K., *J. Catal.*, 1996, vol. 161, no. 1, p. 178.
29. Niwa, Y. and Aika, K., *J. Catal.*, 1996, vol. 162, no. 1, p. 138.
30. Krylov, O.V., *Problemy kinetiki i kataliza* (Problems of Kinetics and Catalysis), Krylov, O.V., Ed., 1973, vol. 15, p. 85.
31. Topchieva, K.V., Loginov, A.Yu., Kreisberg, V.A., and Kostikov, S.V., *Sovremennye problemy fizicheskoi khimii* (Modern Problems of Physical Chemistry), 1975, vol. 8, p. 268.
32. Butyagin, P.Yu., *Usp. Khim.*, 1984, vol. 53, no. 11, p. 1769.
33. Stone, F.S. and Zecchina, A., *Proceedings of VI International Congress of Catalysis, 1976*, Preprint A-8.
34. Tench, A.J., *J. Chem. Soc., Faraday Trans. 1*, 1983, vol. 79, no. 8, p. 1881.

35. Tanaka, K. and Ozaki, A., *J. Catal.*, 1967, vol. 8, no. 1, p. 1.
36. Brown, M.E., Dollimore, D., and Galwey, A.K., *Reactions in the Solid State*, Amsterdam: Elsevier, 1980.
37. L'vov, B.V. and Ugolkov, V.L., *Thermochim. Acta*, 2004, vol. 409, p. 13.
38. Dzis'ko, V.A., Tarasova, D.V., and Karnaukhov, A.P., *Fiziko-khimicheskie osnovy sinteza okisnykh katalizatorov* (Physicochemical Principles of the Synthesis of Oxide Catalysts), Novosibirsk: Nauka, 1978.
39. Dzis'ko, V.A., Ivanova, A.S., Plyasova, L.M., and Ketchik, S.V., *Izv. Akad. Nauk SSSR, Ser. Khim.*, 1978, no. 5, p. 983.
40. Ivanova, A.S., Dzis'ko, V.A., and Ketchik, S.V., *Zh. Neorg. Khim.*, 1980, vol. 25, no. 9, p. 2330.
41. Ivanova, A.S., Pugach, M.M., Moroz, E.M., Litvak, G.S., Kryukova, G.S., Mastikhin, V.M., and Krivoruchko, O.P., *Izv. Akad. Nauk SSSR, Ser. Khim.*, 1989, no. 10, p. 2169.
42. Ivanova, A.S., Moroz, B.L., Litvak, G.S., and Okkel', L.G., *Neorg. Mater.*, 1998, vol. 34, no. 4, p. 432.
43. Jost, H., Braun, M., and Carius, Ch., *Solid State Ionics*, 1997, vols. 101–103, p. 221.
44. Thoms, H., Epple, M., Viebrock, H., and Reller, A., *J. Mater. Chem.*, 1995, vol. 5, p. 589.
45. Thoms, H., Epple, M., and Reller, A., *Solid State Ionics*, 1997, vols. 101–103, p. 79.
46. Hartman, M., Trinke, O., Svoboda, K., and Kocurek, J., *Chem. Eng. Sci.*, 1994, vol. 49, no. 8, p. 1209.
47. Aramendia, M.A., Borau, V., Jimenez, C., Marinas, J.M., Ruiz, J.R., and Urbano, F.J., *Appl. Catal., A*, 2003, vol. 244, p. 207.
48. Bradley, D.C., *Chem. Rev.*, 1989, vol. 89, p. 1317.
49. Caulton, K.G. and Hubert-Pfaltzgraf, L.G., *Chem. Rev.*, 1990, vol. 90, p. 969.
50. Utamapanya, S., Klabunde, K.J., and Schlup, J.R., *Chem. Mater.*, 1991, vol. 3, p. 175.
51. Diao, Y., Walawender, W.P., Sorensen, Ch.M., Klabunde, K.J., and Ricker, T., *Chem. Mater.*, 2002, vol. 14, p. 362.
52. Men', A.N., Vorob'ev, Yu.P., and Chufarov, G.I., *Fiziko-khimicheskie svoistva nestekhiometricheskikh oksidov* (Physicochemical Properties of Nonstoichiometric Oxides), Leningrad: Khimiya, 1973.
53. Kus, S., Otremba, M., Torz, A., and Taniewski, M., *Appl. Catal., A*, 2002, vol. 230, nos. 1–2, p. 263.
54. Anderson, P.J. and Morgan, P.L., *Trans. Faraday Soc.*, 1964, vol. 60, p. 930.
55. Klevtsov, P.V. and Sheina, L.P., *Neorg. Mater.*, 1965, vol. 1, no. 12, p. 2219.
56. Ivanova, A.S., Kalyuzhnaya, E.S., Litvak, G.S., Moroz, E.M., Yunusov, S.M., Lenenko, V.S., Moroz, B.L., Shur, V.B., and Likholobov, V.A., *Kinet. Katal.*, 2004, vol. 45, no. 4, p. 574.
57. Ivanova, A.S., Moroz, E.M., and Litvak, G.S., *Kinet. Katal.*, 1992, vol. 33, nos. 5–6, p. 1208.
58. Orlovskii, V.P. and Chudinova, N.N., *Soedineniya redkozemel'nykh elementov* (Compounds of Rare-Earth Elements), Moscow: Nauka, 1984.
59. *ASTM Diffraction Data Cards and Alphabetical and Grouped Numerical Index of X-ray Diffraction Data*, Philadelphia: ASTM, 1967.
60. Serebrennikov, V.V. and Alekseenko, L.A., *Kurs khimii redkozemel'nykh elementov* (Chemistry of Rare-Earth Elements), Tomsk: Tomsk. Gos. Univ., 1963.
61. Reznitskii, L.A., *Zh. Fiz. Khim.*, 1990, vol. 64, no. 2, p. 561.
62. Leonov, A.I., *Vysokotemperaturnaya khimiya kislorodnykh soedinenii tseriya* (High-Temperature Chemistry of Oxygen Compounds of Cerium), Leningrad: Nauka, 1970.
63. *JCPDS File*, 28-271.
64. *Spravochnik khimika* (Chemist's Handbook), Nikol'skii, B.P., Ed., Leningrad: Khimiya, 1971, p. 381.
65. Voronkov, A.A., Shumyatskaya, N.G., and Pyatenko, Yu.A., *Kristallokhimiya mineralov tsirkoniya i ikh iskusstvennye analogi* (Zirconium Minerals: Crystal Chemistry and Artificial Analogues), Moscow: Nauka, 1978.
66. Zachariasen, W., *Z. Phys. Chem.*, 1926, vol. 123, p. 134.
67. Bevan, D.J.M., *J. Inorg. Nucl. Chem.*, 1955, vol. 1, nos. 1–2, p. 49.
68. Grzybek, T. and Baerns, M., *J. Catal.*, 1991, vol. 129, p. 106.
69. Mariscal, R., Soria, J., Pena, M.A., and Fierro, J.L.G., *J. Catal.*, 1994, vol. 147, p. 535.
70. Mariscal, R., Pena, M.A., and Fierro, J.L.G., *Appl. Catal., A*, 1995, vol. 131, p. 243.
71. Martin, C., Martin, I., and Rives, V., *J. Mol. Catal.*, 1992, vol. 73, p. 51.
72. Szollosi, G. and Bartok, M., *J. Mol. Struct.*, 1999, vol. 482, p. 13.
73. Paukshtis, E.A., *Infrakrasnaya spektroskopiya v geterogennom kislotno-osnovnom katalize* (Infrared Spectroscopy in Heterogeneous Acid–Base Catalysis), Novosibirsk: Nauka, 1992.
74. Yu, L., Li, W., Ducarme, V., Mirodatos, C., and Martin, G.A., *Appl. Catal., A*, 1998, vol. 175, p. 173.
75. Yunusov, S.M., Kalyuzhnaya, E.S., Mahapatra, H., Puri, V.K., Likholobov, V.A., and Shur, V.B., *J. Mol. Catal. A*, 1999, vol. 139, nos. 2–3, p. 219.
76. Yunusov, S.M., Likholobov, V.A., and Shur, V.B., *Appl. Catal., A*, 1997, vol. 158, nos. 1–2, p. L35.